Journal of Materials Chemistry B

ROYAL SOCIETY OF CHEMISTRY

PAPER

View Article Online
View Journal | View Issue

Cite this: J. Mater. Chem. B, 2023, 11, 5537

Promoting photothermal antibacterial activity through an excited-state intramolecular proton transfer process†

Wanni Yao,‡[a] Tian Deng,‡[b] Arui Huang,‡[a] Yufeng Zhang, *[b] Qianqian Li*[a] and Zhen Li *[ac]

Received 7th December 2022,
Accepted 8th February 2023

DOI: 10.1039/d2tb02664c

rsc.li/materials-b

The construction of an efficient photothermal antibacterial platform is a promising strategy for the treatment of drug-resistant bacterial infections. Herein, through the introduction of excited-state intramolecular proton transfer to promote the photothermal effect, *N*-(2,4-dihydroxybenzylidene)-4-aminophenol (DOA)–polyvinyl alcohol (PVA) systems (DPVA) can reach 55 °C within 10 s under irradiation. They show superior antibacterial behavior against drug-resistant bacteria and a therapeutic effect on infected skin wounds with only 100 s of irradiation, much faster than those of reported photothermal materials (5–10 min). This work provides a convenient approach to fabricate broad-spectrum antibacterial wound dressings for treating bacteria-infected wounds, greatly contributing to the design and applications of photothermal antibacterial platforms.

Introduction

The contamination from bacteria and microbes is one of the biggest public health problems, on which, scientists have been working for many years.[1–4] However, traditional antibacterial drugs or therapies are heavily dependent on the use of antibiotics with the mutations of bacteria, resulting in drug resistance.[5–8] This dilemma has prompted scientists to develop more effective antibacterial materials and protocols, including antibacterial peptides, photodynamic therapy, photothermal therapy (PTT), and so on.[9–16] Among the various photothermal antibacterial materials, antibacterial hydrogels have received increasing attention in biomedicine, due to their unique physicochemical properties, excellent biocompatibility, and wide range of adaptability.[17,18] Moreover, the thermal effect can only be produced in a wound dressing with PTT hydrogel reagents under irradiation, which exhibits less damage to the surrounding healthy tissue.[19,20] Generally, *in vitro* diagnosis and treatment can be achieved using hydrogel acting dressings, which are mainly composed of photothermal reagents and polymer substrates.

For photothermal reagents, the thermal effect *via* non-radiative transitions of excited states has emerged recently (Fig. 1A).[21–27] Since it is considered as a negative effect on the luminescence properties of organic materials, some strategies can be borrowed from luminescence materials to promote the photothermal effect, including introduction of molecular rotors and flexible alkyl chains, and the dispersion of photothermal agents in liquid media.[22,23,28–33] Generally, the photothermal effect can be improved by the accelerated molecular motions at the excited states. Excited state proton transfer (ESIPT) is a photochemical process which has high time-domain resolution, proceeding in picosecond time scales ($<10^{12}$ s^{-1}) (Fig. 1A).[34–39] The proton transfer rate (k_{PT} ~ 10^{12} s^{-1}) is at least one order of magnitude higher than that of the vibrational relaxation of the chromophore, *e.g.*, C=C stretching of the phenyl ring (k_{vr} ~ 10^{11} s^{-1}).[40,41] Taking 2-hydroxybenzylideneaniline (OA) as a typical example, the extremely low quantum yield (1.08–3.40%) indicated severe non-radiative transitions under photoexcitation (Table S1, ESI†).[42–46] It was mainly due to the rapid ESIPT and *trans–cis* isomerization, contributing to the promoted photothermal effect. Apart from the antibacterial agents with the photothermal effect, the substrate is also crucial to the antibacterial activity. Among various hydrogels, the polyvinyl alcohol (PVA) hydrogel

[a] Hubei Key Lab on Organic and Polymeric Opto-Electronic Materials, TaiKang Center for Life and Medical Sciences, Sauvage Center for Molecular Sciences, Department of Chemistry, Wuhan University, Wuhan, 430072, China. E-mail: liqianqian@whu.edu.cn, lizhen@whu.edu.cn
[b] State Key Laboratory Breeding Base of Basic Science of Stomatology (Hubei-MOST), Key Laboratory of Oral Biomedicine Ministry of Education, School and Hospital of Stomatology, Wuhan University, Wuhan, 430079, P. R. China. E-mail: zyf@whu.edu.cn
[c] Institute of Molecular Aggregation Science, Tianjin University, Tianjin, 300072, China

† Electronic supplementary information (ESI) available. CCDC 2222100. For ESI and crystallographic data in CIF or other electronic format see DOI: https://doi.org/10.1039/d2tb02664c

‡ These authors contributed equally.

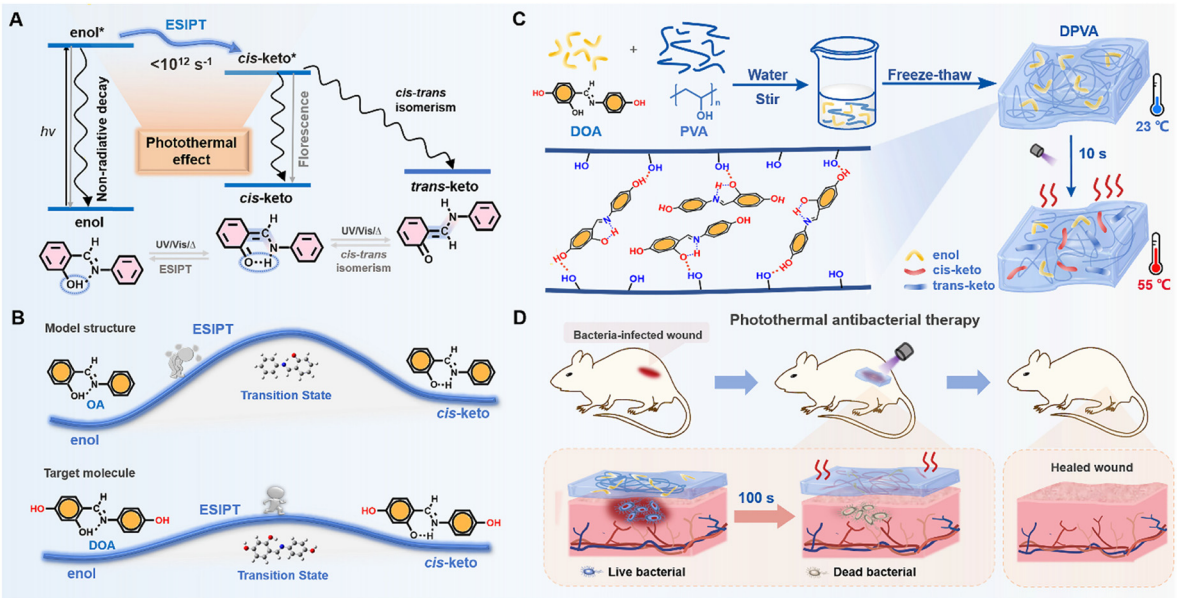

Fig. 1 Schematic illustration of design and fabrication of DPVA hydrogel and its application as a photothermal antibacterial platform for wound dressing. (A) Mechanisms of excited-state intramolecular proton transfer (ESIPT) and *cis–trans* isomerization of *N*-salicylidene aniline. (B) The molecular structures of OA (module molecule) and DOA (target molecule), and energy barrier from the enol to the *cis*–keto form. (C) The fabrication of the DPVA hydrogel and interactions between the DOA and the PVA matrix. (D) The application of the DPVA hydrogel as a photothermal antibacterial platform for wound dressing.

has become the most widely used polymer for hydrogel dressings, because of its low cost, non-toxicity, high water absorption, and excellent biocompatibility.[47–50] Moreover, plentiful hydroxyl groups can interact with antibacterial agents through van der Waals forces, hydrogen bonding, *etc.*, which can avoid the possible phase separation and benefit the building of supramolecular assemblies in the corresponding doped systems.

Thus, the introduction of anils as antibacterial agents into PVA hydrogels should be a good choice to achieve the rapid antibacterial therapeutic effect. Moreover, based on the model molecule of OA with the ESIPT effect, two additional hydroxyl moieties have been incorporated into the formation of *N*-(2,4-dihydroxybenzylidene)-4-aminophenol (DOA) as the target, with the aim to increase interactions between photothermal reagents and substrates using multiple hydrogen bonds (Fig. 1B). Due to the electron-donating effect of hydroxyl units in DOA, the lower energy barrier (Fig. 1B and Fig. S1, ESI†) for the ESIPT process and higher molar extinction coefficient (Fig. S2, ESI†) further promoted the photothermal effect,[51,52] which could be partially proved by the lower photoluminescence quantum yields (<4%) (Table S1, ESI†). Under light irradiation, the temperature of DOA-PVA (DPVA) hydrogels increased from room-temperature to 55 °C within 10 s, then to 73 °C within 100 s (Fig. 1C), much faster than those of the reported photothermal materials (5–10 min), contributing to the rapid photothermal antibacterial process (Table S2, ESI†). Accordingly, *in vitro* antibacterial tests showed that DPVA hydrogel had broad-spectrum disinfection capability with an antibacterial rate of about 99% against *Staphylococcus aureus* (*S. aureus*) and *Escherichia coli* (*E. coli*), as well as the ability to treat drug-resistant bacteria against *Methicillin-resistant Staphylococcus aureus* (*MRSA*) and *Enteroinvasive Escherichia coli* (*EIEC*) with a bacterial survival rate of only about 1%. Whole-layer wound healing experiments in mice showed that *MRSA*-induced wound infections could be effectively cured by the DPVA hydrogel within 100 s of irradiation (Fig. 1D).

Results and discussion

The target molecule DOA was synthesized by a condensation reaction and characterized by ^{1}H NMR, ^{13}C NMR, and HRMS spectroscopy and HPLC (Fig. S3–S6, ESI†). The ESIPT process of DOA can be supported by the distinguishing photophysical properties in protic and aprotic solvents (Fig. 2A and B). The maximum absorption wavelengths in aprotic solutions (acetone and acetonitrile) were around 345 nm, which was mainly derived from the enol form. In protic solutions (methanol and ethanol), the enol–keto equilibrium towards the keto form can be obtained, because of the stronger intermolecular hydrogen bonding between the carbonyl group of the keto form and protic solvents, than those between the phenolic oxygen of the enol form and protic solvents.[53,54] Thus, the weak shoulders around 415 nm emerged from the keto isomer. Accordingly, only weak emission at around 420 nm could be observed in aprotic solvents, while the dual fluorescence peaks at 420 nm and 520 nm can be detected in protic solvents, further confirming the formation of the keto isomer.[54,55] The extremely low quantum yields (1.17–5.67%) of DOA in these solvents indicated that the excited state mainly decayed *via* a non-radiative pathway. Moreover, it can be further confirmed by the higher non-radiative transition rates (K_{nr}) of DOA in protic solvents than

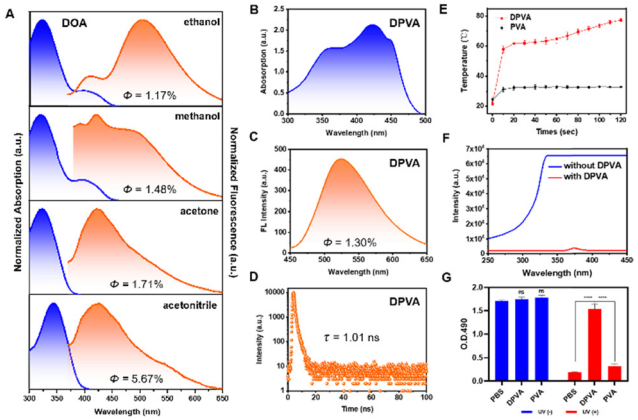

Fig. 2 Photophysical properties and *in vitro* photothermal effect of the DPVA hydrogel. (A) UV-Vis absorption spectra and fluorescence spectra of DOA in different solutions (excitation wavelength: 369 nm for ethanol solution, 383 nm for methanol solution, 373 nm for acetone solution, 350 nm for acetonitrile solution). (B) UV-Vis absorption spectrum, (C) fluorescence spectrum (excitation wavelength: 377 nm) and (D) fluorescence decay of DPVA hydrogel. (E) Photothermal heating curves of PVA and DPVA hydrogel under UV irradiation (average power density is 210 mW cm^{-2}) for 100 s. (F) The light intensity in the UV region with/without DPVA covered. (G) Statistical results of cytocompatibility evaluation through contact with the L929 cells under different conditions.

those in aprotic ones under similar polarity conditions (Fig. S7 and Table S3, ESI†). For instance, K_{nr} of DOA in ethanol and acetone solution with similar dielectric constants are 9.60×10^8 s^{-1} and 8.55×10^8 s^{-1}, respectively, and the larger K_{nr} value in ethanol as the protic solvent is mainly due to the promoted ESIPT process. It can also be confirmed by the larger K_{nr} value of DOA in methanol (7.64×10^8 s^{-1}) than that (6.17×10^8 s^{-1}) in acetonitrile solution. Once DOA is doped into PVA hydrogel, the resultant DOA-PVA (DPVA) hydrogel with a thickness of 1.0 mm exhibited two main absorption peaks: the peak located at about 350 nm was attributed to the enol form of DOA, while that at 415 nm might be due to the keto form. Accordingly, the severe non-radiative transitions of DPVA resulted in the low quantum yields of 1.30% (Fig. 2C), short fluorescence lifetime of 1.01 ns (Fig. 2D) and high K_{nr} of 9.77×10^8 s^{-1}, contributing to the promoted photothermal antibacterial activity. They were mainly attributed to the rapid ESIPT process and *cis–trans* isomerization at the excited state as molecular motions, which could be further confirmed by the light-driven droplet movement experiments (Fig. S8, ESI†).

The morphology of the DPVA hydrogel showed a three-dimensional laminar porous structure with homogeneous round pores (Fig. S9, ESI†). The tensile stress of DPVA was 384 kPa with strain of 196%, and its compressive stress was 1.41 MPa at maximum compressive strain of 80% (Fig. S10, ESI†). These results suggested that DPVA had an appropriate mechanical strength, which could resist external forces without damage. Moreover, the toughness and elastic modulus of DPVA could reach to 465 kJ m^{-3} and 62 kPa, respectively, indicating good elasticity and malleability.

Subsequently, the photothermal properties of DPVA hydrogel were investigated, and the corresponding changes of temperature were recorded and shown in Fig. 2E. Under UV irradiation, the temperature of DPVA hydrogel rose to 55 °C rapidly within 10 s, and finally reached around 73 °C after 100 s. Since the pure PVA hydrogel could only increase about 10 °C under the same conditions, the photothermal effect of DPVA hydrogel was mainly from DOA by rapid molecular motions. Since bacteria can be killed when the temperature exceeds 50 °C, DPVA hydrogel should possess efficient photothermal antibacterial activity. Before the *in vitro* antibacterial experiments, in order to ensure the safety of DPVA hydrogel as an antibacterial material under irradiation, the light intensity in the UV region after passing through the DPVA hydrogel was tested. As shown in Fig. 2F, the strong input UV light became extremely low after passing hydrogel, indicating that the UV light has been shielded by DPVA hydrogel for the strong absorption capacity of DOA in UV region. Also, when the cells treated with DPVA hydrogel under UV light, the L929 cell viability exhibited almost no difference with that at the initial state (Fig. 2G and Fig. S11, ESI†), further confirming the safety of PTT treatment using DPVA hydrogel.

The *in vitro* antibacterial activity of the DPVA hydrogel was investigated by spreading plate experiments of Gram-positive and Gram-negative bacteria after incubation of the DPVA hydrogel at 37 °C. Lots of viable colonies appeared on all Luria-Bertani (LB) agar plates of the blank groups, *i.e.*, direct treatments with PBS, PVA or DPVA hydrogel were almost non-effective on *S. aureus* (Fig. 3A and Fig. S12, ESI†). After 100 s of light irradiation, DPVA hydrogel showed more than 99% bacterial inhibition against *S. aureus* (Fig. 3B). With the aim to confirm the photothermal effect on antibacterial properties, an ice bath was utilized to decrease the surface temperature of

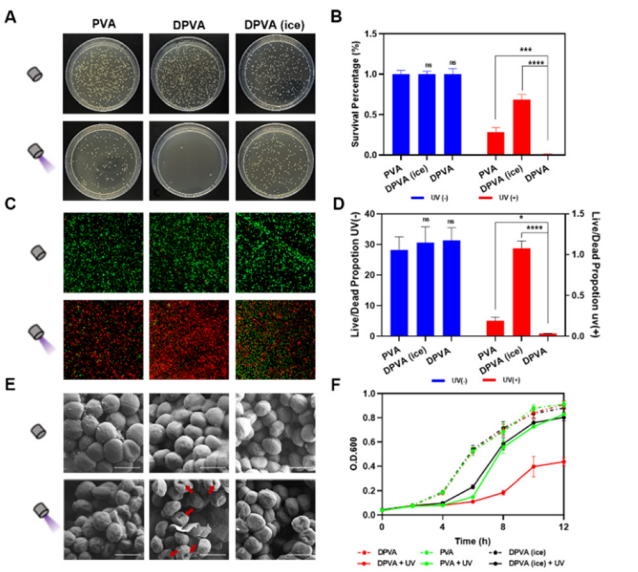

Fig. 3 Antibacterial activity of DPVA hydrogel against *S. aureus*. (A) Pictures of *S. aureus* grown on agar plates and (B) the corresponding inhibition percentage of *S. aureus* with different treatments. (C) Fluorescence microscope image and (D) corresponding proportion of *S. aureus* with different treatments. (E) SEM photographs and (F) growth curve of *S. aureus* with different treatments (red arrows: the wrinkles and holes of bacteria) (scale bar = 1 μm).

DPVA hydrogel. Accordingly, the control group in the presence of an ice bath, showed a very low inhibition rate (31.6%), suggesting that the antibacterial effect decreased sharply upon the elimination of the photothermal effect. Once DOA was removed from DPVA hydrogel, the inhibition rate of PVA hydrogel was less than 75%, which was mainly from UV damage,[56] as proved by the result of the PBS group with irradiation (Fig. S12, ESI†), usually accompanied by DNA lesions. However, for the treatment of DPVA hydrogel with DOA, the UV damage can be shielded by the strong absorbance of DOA in the UV region, which can ensure the safety of antibacterial experiments. Thus, the DPVA hydrogel possessed efficient photothermal antibacterial effect, together with UV shielding properties. When the wound was covered with DPVA hydrogel and irradiated for 100 s, extremely low *E. coli* survival rate could be detected (~1%, Fig. S13, ESI†). Moreover, it showed excellent antibacterial effects against *MRSA* (Fig. S14, ESI†) and *EIEC* (Fig. S15, ESI†) with the antibacterial rate reaching ~99%, as proved from the plate laying experiments, demonstrating the broad-spectrum photothermal antibacterial activity of the DPVA hydrogel.

Subsequently, fluorescence microscope imaging with live/dead staining assay were performed on *S. aureus* (Fig. 3C and D and Fig. S16, ESI†), to confirm the antibacterial effect of DPVA hydrogel at the microscopic level. All bacteria were stained, generally, with live *S. aureus* emitting green fluorescence, and dead *S. aureus* displaying red fluorescence. As shown in Fig. 3C, without light irradiation, all of them exhibited the green fluorescence, indicating almost no sterilization ability. After irradiation, DPVA hydrogel exhibited a significant antibacterial effect, as confirmed by the almost red fluorescence imaging. It is mainly from photothermal properties, as proved by the much weakened antibacterial effect by the decreased surface temperature in the presence of ice. Also, the UV damage could be observed in PVA treatment, resulting in the partial red fluorescence imaging. Live and dead assay analysis also demonstrated the high antibacterial activity of DPVA hydrogel, which was consistent with the results of colony-forming count measurements (Fig. 3D). Moreover, the fluorescence microscope image on *E. coli* exhibited similar phenomena, further confirming the efficient photothermal antibacterial effect of DPVA hydrogel on various bacteria (Fig. S17, ESI†).

On account of the fact that photothermal ablation led to amorphous and wizened change of the bacterial surface, scanning electron microscopy (SEM) was utilized to visualize the morphology of *S. aureus* (Fig. 3E and Fig. S18, ESI†) and *E. coli* (Fig. S19, ESI†) with the different treatment. Without irradiation, all of them showed an intact morphology and smooth surface with almost no damage to bacteria. Under irradiation, slight wrinkles and shrinkage could be observed on the surface of *S. aureus* by the introduction of PVA and DPVA (ice), which still maintained a sound cell structure, indicating an insufficient bactericidal effect. However, in the presence of DPVA hydrogel with irradiation, most of the bacteria showed wrinkles and holes in the visual field, indicating that the bacterial structure was completely disrupted due to the generated high temperature. In addition, the growth curves of bacteria were used to evaluate the proliferation inhibition effect. As shown in Fig. 3F, after *S. aureus* was treated with different hydrogels, the OD600 values increased rapidly within the first 6 h, and then increased slowly into a platform stage, which was similar to that of the control group with PBS treatment (Fig. S20, ESI†). Once the light irradiation was incorporated, the proliferation weakened to different degrees, with the growth in the DPVA hydrogel hindered the most. The arrival of exponential growth phase of *S. aureus* was delayed by around 2 h with the treatment of PVA and DPVA (ice), while it kept a bacteria-resistance condition for another 4 h by DPVA hydrogel. Similar phenomena could be observed in the growth curves of *E. coli* after different treatments (Fig. S21, ESI†). These *in vitro* results exhibited that DPVA was able to inhibit the growth of bacteria, due to the efficient photothermal effect.

Excellent biocompatibility is an important factor for practical application. Accordingly, *in vitro* blood tests were performed to evaluate the biocompatibility of DPVA hydrogel. The negative control (PBS) groups exhibited a clear light yellow colour, while the positive control group (erythrocytes lysis buffer) noticeably turned red, due to complete hemolysis (Fig. S22, ESI†). The supernatants of PVA and DPVA were observed similar to the negative control (PBS) groups. Also, quantitative data visually showed a very low hemolysis rate for PVA hydrogel (0.71%) and the DPVA hydrogel (3.74%), indicating the negligible hemolysis rate of the hydrogel. To further evaluate the cytotoxicity of these hydrogels, direct contact tests between L929 cells and the hydrogels were performed. There was no significant difference in cell viability between PVA, DPVA and PBS groups (Fig. S23, ESI†). It confirmed that DPVA hydrogel was biologically hemocompatible and promising for antibacterial wound dressing applications. Subsequently, the *in vivo* wound healing by DPVA hydrogel was evaluated by using infected wound models. Firstly, the photothermal effect of hydrogels was tested on the epidermis of mice. As shown in Fig. 4A and B, the surface temperature of PVA hydrogel could only increase to 38 °C within 100 s under irradiation, similar to that of the control group (PBS), indicating a weak photothermal effect. Once the abscess area of the mice was treated using DPVA hydrogel, the temperature increased rapidly, reaching up to ~50 °C, which was deemed high enough to destroy the bacteria. Moreover, no significant edema or burns were detected in the infected area, indicating that the temperature was appropriate for the skin.

Therefore, DPVA hydrogel was used as an antibacterial wound dressing for the treatment of infected wounds over a 20 day period. On Day 7, the skin lesions of these mice were measured by the area of wounds to investigate therapeutic efficacy. Upon irradiation, the wound on the mice back with DPVA treatment started healing with no visible pus, and the area of the wound began to decrease, while those with PVA and PBS were still covered by different degrees of pus and the area of the wound was barely reduced (Fig. S24, ESI†). Subsequently, the skin of the infected wound in each group was harvested, and the number of bacteria extracted from the wound tissue

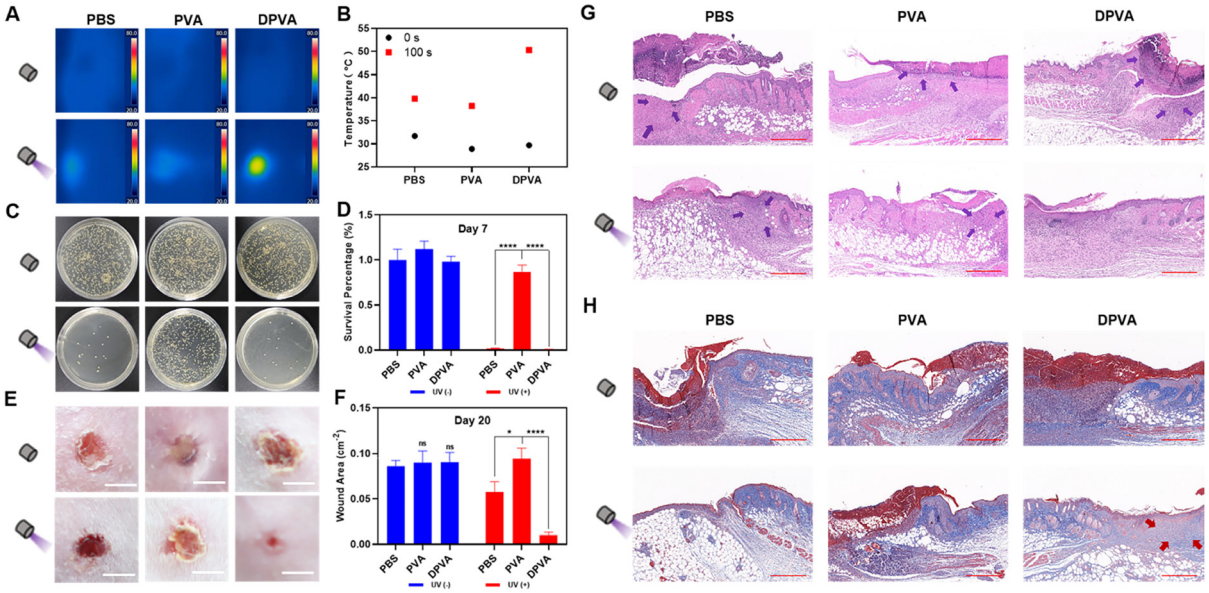

Fig. 4 *In vivo* assessment of antibacterial properties of PVA/DPVA hydrogel. (A) Infrared thermal images and (B) the corresponding temperature elevation at the wound sites in the PBS and hydrogel groups with/without UV irradiation. (C) Pictures of MRSA grown on agar plates and (D) the corresponding inhibition percentage of the MRSA-infected wounds with different treatments at Day 7. (E) Photographs and (F) quantitative analysis of lesion sites of MRSA-infected wounds with different treatments on Day 20 (scale bar = 0.5 cm). (G) H&E staining and (H) Masson's trichrome staining of the skin tissues from the wound edges of MRSA-infected wounds with different treatments on Day 20 (purple arrows: area of inflammation, red arrows: collagen fibers) (scale bar = 500 μm).

supernatant was counted using a plate method to investigate the antibacterial efficacy. As shown in Fig. 4C and D, the number of bacteria decreased to different degrees using these hydrogels under irradiation, and the highest antibacterial efficacy was achieved by DPVA hydrogel with almost no colony forming units, in line with the *in vitro* results, illustrating that DPVA hydrogel was effective for *in vivo* experiment. Furthermore, the histological changes in the skin tissue were evaluated to verify the above therapeutic results. As shown in the hematoxylin & eosin (H&E) stained images on Day 7 (Fig. S25, ESI†), the edges of the wound were fully infiltrated by inflammatory cells without irradiation, indicating almost no therapeutic efficacy in these cases. Once irradiation treatment was introduced, some reduction in inflammatory cells can be observed, especially in the DPVA group, where no apparent inflammation occurred and morphology of normal tissue cells was clearly discernible (Fig. S25, ESI†). The same trends could be also found in Masson staining (Fig. S26, ESI†).

The areas of the wounds by the treatment of hydrogels further decreased on day 20, compared to those of the corresponding group on Day 7. In particular, the wound treated using DPVA hydrogel under irradiation was basically healed with the smallest wound area ($\sim$0.01 cm^{-2}), while those with PVA and PBS treatment were about 0.09 cm^{-2} and 0.06 cm^{-2}, respectively (Fig. 4E and F). The recovery of the PBS group with irradiation was much worse than that of DPVA hydrogel on Day 20, though there were few colony forming units and pus covered on the wound on Day 7. It was presumably because the continuous UV exposure damaged the skin tissues, greatly hindering the recovery of the wound. This result could be further confirmed by the H&E staining (Fig. 4G). It could be obviously observed that the skin treated with the DPVA hydrogel under irradiation was intact, and the new epidermal tissue was obvious, while the deeper epidermal tissue with PBS treatment was still not restored, no matter that the epidermal integrity was recovered. A similar phenomenon could also be observed in Masson staining (Fig. 4H). After irradiation, more collagen fibres appeared in the DPVA group than in other groups. Hence, the DPVA hydrogel is an excellent antibacterial material to treat infection wounds, *via* a rapid photothermal effect to kill bacteria, as well as for the prevention of possible UV damage to skin.

Conclusions

In conclusion, we have successfully constructed an antibacterial platform (DPVA hydrogel) for the efficient treatment of drug-resistant bacterial infections in skin wounds rapidly, which is mainly derived from the photothermal effect of DOA with the increased temperature to 55 °C within 10 s under irradiation. This is the first example in which an ESIPT process as non-radiative transitions was utilized to promote the photothermal effect, thus providing a new way to develop antibacterial materials with rapid response and convenient fabrication. Moreover, further research on photothermal antibacterial treatment under Xe lamp or visible light is still on the way, which could be realized by incorporation with the other extended conjugated systems,[57–59] and the feasibility has been proved by the primary experiments.

Author contributions

Z. L. and Q. L. conceived this research. W. Y. and A. H. designed and synthesized the target molecules. W. Y. developed and fabricated the hydrogel and completed the material characterization tests. W. Y. and T. D. conducted biological experiments under the supervision of Y. Z., Q. L. and Z. L. A. H. carried out theoretical calculations. All authors contributed to writing the manuscript.

Conflicts of interest

There are no conflicts to declare.

Acknowledgements

This work was supported by the National Natural Science Foundation of China (22235006, 51973162 and 22122504), the Excellent Youth Foundation of Hubei Scientific Committee (2020CFA084), and the Fundamental Research Funds for the Central Universities (2042202kf0031). All animal studies were performed according to the guidelines and the overall project protocols were approved by the Ethics Committee of the School and Hospital of Stomatology, Wuhan University (A31/2020). We thank Prof. Jinping Zhou for providing the platform with tensile and compression stress–strain measurements. We are grateful to National Supercomputing Center in Shenzhen for theoretical calculation support.

Notes and references

1 Z. Wang, B. Koirala, Y. Hernandez, M. Zimmerman, S. Park, D. S. Perlin and S. F. Brady, *Nature*, 2022, **601**, 606–611.
2 T. Deng, H. Zhao, M. Shi, Y. Qiu, S. Jiang, X. Yang, Y. Zhao and Y. Zhang, *Small*, 2019, **15**, 1902647.
3 H. Tang, X. Qu, W. Zhang, X. Chen, S. Zhang, Y. Xu, H. Yang, Y. Wang, J. Yang, W.-E. Yuan and B. Yue, *Adv. Mater.*, 2022, **34**, 2107300.
4 J. Gu, Z. Li and Q. Li, *Coord. Chem. Rev.*, 2023, **475**, 214872.
5 X. Qi, Y. Huang, S. You, Y. Xiang, E. Cai, R. Mao, W. Pan, X. Tong, W. Dong, F. Ye and J. Shen, *Adv. Sci.*, 2022, **9**, 2106015.
6 X. Zhao, H. Tang and X. Jiang, *ACS Nano*, 2022, **16**, 10066–10087.
7 S. Hussain, J. Joo, J. Kang, B. Kim, G. B. Braun, Z.-G. She, D. Kim, A. P. Mann, T. Mölder, T. Teesalu, S. Carnazza, S. Guglielmino, M. J. Sailor and E. Ruoslahti, *Nat. Biomed.l Eng.*, 2018, **2**, 95–103.
8 Y.-J. Zou, S.-S. He and J.-Z. Du, *Chin. J. Polym. Sci.*, 2018, **36**, 1239–1250.
9 Y. Liu, Y. Xiao, Y. Cao, Z. Guo, F. Li and L. Wang, *Adv. Funct. Mater.*, 2020, **30**, 2003196.
10 Y. Liu, P. Bhattarai, Z. Dai and X. Chen, *Chem. Soc. Rev.*, 2019, **48**, 2053–2108.
11 Y. Qiu, S. Yu, Y. Wang, L. Xiao, L. Pei, Y. Pu and Y. Zhang, *Biomater. Sci.*, 2022, **10**, 1995–2005.
12 L. Zhang, Y. Wang, J. Wang, Y. Wang, A. Chen, C. Wang, W. Mo, Y. Li, Q. Yuan and Y. Zhang, *ACS Appl. Mater. Interfaces*, 2019, **11**, 300–310.
13 N. Yang, C. Cao, H. Li, Y. Hong, Y. Cai, X. Song, W. Wang, X. Mou and X. Dong, *Small Struct.*, 2021, **2**, 2100110.
14 G. Cheng, W. Zong, H. Guo, F. Li, X. Zhang, P. Yu, F. Ren, X. Zhang, X. Shi, F. Gao, J. Chang and S. Wang, *Adv. Mater.*, 2021, **33**, 2100398.
15 N. Dey, A. Ali, M. Kamra and S. Bhattacharya, *J. Mater. Chem. B*, 2019, **7**, 986–993.
16 N. Dey, D. Biswakarma, A. Bajpai, J. N. Moorthy and S. Bhattacharya, *ChemPhysChem*, 2019, **20**, 881–889.
17 S. Chen, F. Tang, L. Tang and L. Li, *ACS Appl. Mater. Interfaces*, 2017, **9**, 20895–20903.
18 R. Chang and X. Yan, *Small Struct.*, 2020, **1**, 2000068.
19 Z. Cao, Y. Luo, Z. Li, L. Tan, X. Liu, C. Li, Y. Zheng, Z. Cui, K. W. K. Yeung, Y. Liang, S. Zhu and S. Wu, *Macromol. Biosci.*, 2021, **21**, 2000252.
20 J. Xu, X. Yang, X. Tang and M.-X. Zhao, *J. Mater. Chem. C*, 2022, **10**, 16283–16293.
21 C. Xu, R. Ye, H. Shen, J. W. Y. Lam, Z. Zhao and B. Zhong Tang, *Angew. Chem., Int. Ed.*, 2022, **61**, e202204604.
22 D. Xi, M. Xiao, J. Cao, L. Zhao, N. Xu, S. Long, J. Fan, K. Shao, W. Sun, X. Yan and X. Peng, *Adv. Mater.*, 2020, **32**, 1907855.
23 H. Li, H. Wen, Z. Zhang, N. Song, R. T. K. Kwok, J. W. Y. Lam, L. Wang, D. Wang and B. Z. Tang, *Angew. Chem., Int. Ed.*, 2020, **59**, 20371–20375.
24 X. Cai, J. Liu, W. H. Liew, Y. Duan, J. Geng, N. Thakor, K. Yao, L.-D. Liao and B. Liu, *Mater. Chem. Front.*, 2017, **1**, 1556–1562.
25 F. Lv, X. Fan, D. Liu and F. Song, *Acta Biomater.*, 2022, **149**, 16–29.
26 F. Liu, Q. Liao, J. Wang, Y. Gong, Q. Dang, W. Ling, M. Han, Q. Li and Z. Li, *Sci. China: Chem.*, 2020, **63**, 1435–1442.
27 G. Feng and B. Liu, *Small*, 2016, **12**, 6528–6535.
28 D. Wang, M. M. S. Lee, W. Xu, G. Shan, X. Zheng, R. T. K. Kwok, J. W. Y. Lam, X. Hu and B. Z. Tang, *Angew. Chem., Int. Ed.*, 2019, **58**, 5628–5632.
29 S. Liu, X. Zhou, H. Zhang, H. Ou, J. W. Y. Lam, Y. Liu, L. Shi, D. Ding and B. Z. Tang, *J. Am. Chem. Soc.*, 2019, **141**, 5359–5368.
30 Z. Zhao, C. Chen, W. Wu, F. Wang, L. Du, X. Zhang, Y. Xiong, X. He, Y. Cai, R. T. K. Kwok, J. W. Y. Lam, X. Gao, P. Sun, D. L. Phillips, D. Ding and B. Z. Tang, *Nat. Commun.*, 2019, **10**, 768.
31 J. Li, J. Wang, J. Zhang, T. Han, X. Hu, M. M. S. Lee, D. Wang and B. Z. Tang, *Adv. Mater.*, 2021, **33**, 2105999.
32 Y. Fan, M. Han, A. Huang, Q. Liao, J. Tu, X. Liu, B. Huang, Q. Li and Z. Li, *Mater. Horiz.*, 2022, **9**, 368–375.
33 Q. Li and Z. Li, *Acc. Chem. Res.*, 2020, **53**, 962–973.
34 V. S. Padalkar and S. Seki, *Chem. Soc. Rev.*, 2016, **45**, 169–202.
35 A. P. Demchenko, K.-C. Tang and P.-T. Chou, *Chem. Soc. Rev.*, 2013, **42**, 1379–1408.
36 A. Huang, J. Hu, M. Han, K. Wang, J. L. Xia, J. Song, X. Fu, K. Chang, X. Deng, S. Liu, Q. Li and Z. Li, *Adv. Mater.*, 2021, **33**, 2005249.

37 N. Dey and S. Bhattacharya, *Chem. Commun.*, 2017, **53**, 5392–5395.
38 N. Dey and S. Bhattacharya, *ACS Sustainable Chem. Eng.*, 2021, **9**, 17078–17084.
39 N. Dey, *ChemistrySelect*, 2020, **5**, 6823–6827.
40 K. Ding, S. J. Courtney, A. J. Strandjord, S. Flom, D. Friedrich and P. F. Barbara, *J. Phys. Chem.*, 1983, **87**, 1184–1188.
41 R. S. Becker, C. Lenoble and A. Zein, *J. Phys. Chem.*, 1987, **91**, 3509–3517.
42 M. E. Kletskii, A. A. Millov, A. V. Metelitsa and M. I. Knyazhansky, *J. Photochem. Photobiol., A*, 1997, **110**, 267–270.
43 M. Ziółek, J. Kubicki, A. Maciejewski, R. Naskręcki and A. Grabowska, *Phys. Chem. Chem. Phys.*, 2004, **6**, 4682–4689.
44 R. D. Kieda, A. D. Dunkelberger, A. S. Case and F. F. Crim, *J. Phys. Chem. B*, 2017, **121**, 835–842.
45 J.-W. Hu, H.-Y. Tsai, S.-K. Fang, C.-W. Chang, L.-C. Wang and K.-Y. Chen, *Dyes Pigm.*, 2017, **145**, 493–504.
46 S. Pijeau, D. Foster and E. G. Hohenstein, *J. Phys. Chem. A*, 2018, **122**, 5555–5562.
47 J. Wang, M. Zhang, S. Han, L. Zhu and X. Jia, *J. Mater. Chem. C*, 2022, **10**, 15565–15572.
48 Z. Pan, H. Ye and D. Wu, *APL Bioeng.*, 2021, **5**, 011504.
49 Y. Zhang, M. Jiang, Y. Zhang, Q. Cao, X. Wang, Y. Han, G. Sun, Y. Li and J. Zhou, *Mater. Sci. Eng. Carbon*, 2019, **104**, 110002.
50 B. Zhu, E. W. C. Chan, S. Y. Li, X. Sun and J. Travas-Sejdic, *J. Mater. Chem. C*, 2022, **10**, 14882–14891.
51 X. Li, Q. Wang, L. Song, J. Zhao and B. Jin, *Spectrochim. Acta, Part A*, 2022, **279**, 121377.
52 M. Ni, X. Liang and H. Fang, *J. Phys. Org. Chem.*, 2021, **34**, e4216.
53 S. Nagaoka, A. Itoh, K. Mukai and U. Nagashima, *J. Phys. Chem.*, 1993, **97**, 11385–11392.
54 M. Ziółek, G. Burdziński, K. Filipczak, J. Karolczak and A. Maciejewski, *Phys. Chem. Chem. Phys.*, 2008, **10**, 1304–1318.
55 M. Ziółek, J. Kubicki, A. Maciejewski, R. Naskręcki and A. Grabowska, *J. Chem. Phys.*, 2006, **124**, 124518.
56 G. P. Pfeifer, *Genome Instab. Dis.*, 2020, **1**, 99–113.
57 Y. Fan, S. Liu, M. Wu, L. Xiao, Y. Fan, M. Han, K. Chang, Y. Zhang, X. Zhen, Q. Li and Z. Li, *Adv. Mater.*, 2022, **34**, 2201280.
58 Q. Zhang, Y. Fan, Q. Liao, C. Zhong, Q. Li and Z. Li, *Sci. China: Chem.*, 2022, **65**, 918–925.
59 J. Wang, Q. Dang, Y. Gong, Q. Liao, G. Song, Q. Li and Z. Li, *CCS Chem.*, 2021, **3**, 274–286.